Probabilistic assessment of landslide tsunami hazard for the northern Gulf of Mexico

A. Pampell-Manis[1], J. Horrillo[1], Y. Shigihara[2], and L. Parambath[1]

[1]Department of Maritime Systems Engineering, Texas A&M University at Galveston, Galveston, Texas, USA, [2]Department of Civil and Environmental Engineering, National Defense Academy, Yokosuka, Japan

Abstract The devastating consequences of recent tsunamis affecting Indonesia and Japan have prompted a scientific response to better assess unexpected tsunami hazards. Although much uncertainty exists regarding the recurrence of large-scale tsunami events in the Gulf of Mexico (GoM), geological evidence indicates that a tsunami is possible and would most likely come from a submarine landslide triggered by an earthquake. This study customizes for the GoM a first-order probabilistic landslide tsunami hazard assessment. Monte Carlo Simulation (MCS) is employed to determine landslide configurations based on distributions obtained from observational submarine mass failure (SMF) data. Our MCS approach incorporates a Cholesky decomposition method for correlated landslide size parameters to capture correlations seen in the data as well as uncertainty inherent in these events. Slope stability analyses are performed using landslide and sediment properties and regional seismic loading to determine landslide configurations which fail and produce a tsunami. The probability of each tsunamigenic failure is calculated based on the joint probability of slope failure and probability of the triggering earthquake. We are thus able to estimate sizes and return periods for probabilistic maximum credible landslide scenarios. We find that the Cholesky decomposition approach generates landslide parameter distributions that retain the trends seen in observational data, improving the statistical validity and relevancy of the MCS technique in the context of landslide tsunami hazard assessment. Estimated return periods suggest that probabilistic maximum credible SMF events in the north and northwest GoM have a recurrence of 5000–8000 years, in agreement with age dates of observed deposits.

1. Introduction

It is relatively well understood that damaging tsunamis can be triggered by large earthquakes, as seen by the devastating 2004 Indian Ocean and 2011 Japan tsunamis. These recent catastrophic events have prompted a more full-scale assessment of tsunami hazard along coastal regions, even in areas with an apparent low risk and/or lack of a comprehensive historical tsunami record. Of particular interest to the proposed study is the tsunami hazard potential within the Gulf of Mexico (GoM) and threats to the region's coastal communities as well as the large-scale shipping and natural resource exploration and production industries. In accordance with the recent focus on hazard assessment in low-risk areas, GoM coasts have been included in the United States Tsunami Warning System since January 2005 in order to enable local emergency management to act in response to tsunami warnings.

While the GoM is certainly at lower risk for tsunami hazards than other U.S. coastal areas, investigations carried out by the U.S. Geological Survey (USGS) and the National Tsunami Hazard Mitigation Program (NTHMP) [*ten Brink et al.*, 2009a] revealed that three small tsunami events occurred within the GoM in the twentieth century. The first was a small indeterminate-amplitude tsunami wave generated by a seismic event west of Puerto Rico and detected by a Galveston, TX, tide gauge station in October 1918, though there is some confusion regarding the exact date. The second occurred on 2 May 1922 when a 0.64 m (2.1 ft) amplitude wave was recorded at a Galveston tide gauge station, most likely resulting from an event local to the GoM and Galveston. The third event resulted in seismic seiche waves originating from the 27 March 1964 Gulf of Alaska earthquake, and 0.18 m (0.6 ft) amplitude waves were recorded at a Freeport, TX, tide gauge station.

In general, possible tsunami sources impacting the GoM are local submarine landslides and possibly earthquakes originating from the Caribbean plate faults. However, preliminary modeling of potential tsunami

sources outside the GoM by *Knight* [2006] indicated that they are a very low threat and may not significantly impact GoM coastal communities or infrastructure. Thus, as reported by *ten Brink et al.* [2009a], local submarine landslides in the GoM are considered to be the primary potential source of tsunami generation in the GoM.

Submarine landslides or submarine mass failures (SMFs) can, in general, occur in confined water bodies, near island formations, and along continental slopes. Tsunami generation by these slides depends on the geological characteristics of the sloping sediment and the triggering mechanism affecting the region. Common mechanisms to initiate an underwater landslide and the ensuing tsunami are earthquakes, overpressure due to rapid deposition of soil sediments, presence of weak soil layers, wave loading on the seabottom sediments by storms or hurricanes, buildup of excess pore water pressure, gas hydrate dissociation by change of temperature or pressure, groundwater seepage, and slope oversteepening [*Hampton and Locat*, 1996; *Locat and Lee*, 2002; *Masson et al.*, 2006]. The GoM is a geologically diverse and unique environment where many of these mechanisms are present, including rapid sedimentation, salt movement, and repeated wave loading from storms. Such processes surely contribute to slope instability and may cause slope failures in and of themselves; however, most large-scale submarine landslides, while perhaps being preconditioned to failure by these processes, have been initiated by earthquakes [*Masson et al.*, 2006; *ten Brink et al.*, 2009b; *Dugan and Stigall*, 2010; *Harbitz et al.*, 2014]. Thus, across the low-angle GoM continental shelf/slope, earthquakes are expected to be the most likely trigger of slope failures which are massive enough and which occur on a short enough time scale (i.e., instantaneously) to produce a tsunami wave.

Several recent moderate-sized earthquakes have occurred in the GoM, including a M5.3 seismic event (likely gravity-driven) that occurred 10 February 2006 [*Dellinger and Blum*, 2009] and a M5.9 earthquake on 10 September 2006 (significantly large for this region). While these events did not produce a noticeable tsunami or submarine landslide (though the 10 February 2006 event shows evidence of sediment dislocation at depth [*Dellinger and Blum*, 2009]), even low-magnitude earthquakes such as these have the potential to trigger slope failure along passive continental margins. *Ten Brink et al.* [2009b] showed that earthquake magnitudes as small as 5.5 and located very near the western Atlantic continental slope could trigger slope failures large enough to generate tsunamis. Additionally, *Stigall and Dugan* [2010] found that a magnitude 5.0 earthquake near the Ursa region in the GoM could have initiated slope failure. Thus, while the GoM tsunami warning threshold is currently set at magnitude 6.5 (7.0 if the earthquake is located in deep water and farther than 75 km from the continental slope) [*Whitmore et al.*, 2009], even low-magnitude earthquakes which occur near the continental slope have the potential to trigger submarine landslides in the GoM.

Tsunamis generated by SMF events are distinctly different from those generated by earthquakes. Because of the smaller spatial scale of landslides as compared to fault slip sources, waves from SMF sources are generated in a more radial direction than those from earthquakes and exhibit shorter wavelengths and stronger dispersion. Additionally, the longer time scales and large vertical displacements of the landslide source motion lead to more nonlinear behavior in wave generation as compared to earthquakes. Landslide tsunami can also produce much more localized damage than those generated by earthquakes. Their threat to life and property has been increasingly realized over the past century. In 1929, in Grand Banks, an earthquake-induced underwater landslide produced tsunami waves of 3–8 m which killed 28 people along the coast of Newfoundland [*Cranford*, 2000]. The 1964 Alaska earthquake generated multiple local submarine landslides, including one near old Valdez which produced waves 4.5–7.6 m high (some localized up to 12 m) [*Brown*, 1964] and resulted in 33 deaths at old Valdez—more than those caused by the earthquake at any other location. Even greater devastation was seen with the 1998 Papua New Guinea landslide tsunami, which produced waves up to 15 m high, took over 2200 lives, and destroyed three villages [*Tappin et al.*, 2008]. Several groups subsequently refocused attention on submarine landslides and the potential for tsunami generation in both experimental and numerical studies, including *Grilli and Watts* [1999], *Lynett and Liu* [2002], *Liu et al.* [2005], *ten Brink et al.* [2006], *Sue et al.* [2006], *Hornbach et al.* [2008], *Fritz et al.* [2009], *Geist et al.* [2009], *Grilli et al.* [2009], *Horrillo et al.* [2013], *Ma et al.* [2013], and *López-Venegas et al.* [2015].

Although a massive underwater landslide in the GoM is considered a potential hazard, the probability of such an event is quite low [*Dunbar and Weaver*, 2008]. The probability of occurrence is related to large ancient landslides which, based on the limited availability of age information for large-scale submarine failures, were probably active prior to 7000 years ago when large quantities of sediments were emptied into the GoM [*ten Brink et al.*, 2009a]. However, sediments continue to empty into the GoM mainly from the

Mississippi River. This sediment supply contributes to slope steepening and the increase of excess pore water pressure in the underlying soils, which may lead to slope instabilities and earthquake-induced large-scale tsunamigenic failures, as discussed above. In addition, the unique basin geometry of the GoM makes even unlikely tsunami events potentially hazardous to the entire Gulf Coast. Waves tend to refract along continental slopes and shelf breaks, and given the curved geomorphology of the GoM shelf and the concave shape of the coastline, any outgoing propagating wave could potentially affect the coast immediately adjacent to the landslide source as well as the opposite coast. Thus, while offshore the eastern and western U.S. coasts, the primary threat from a local SMF source is the backgoing tsunami wave, affecting a localized region in the opposite direction of slide motion, in the GoM both backgoing and outgoing waves from an SMF event are a potential inundation threat to coastal communities a greater distance apart than their counterparts on the eastern or western U.S. coasts.

Given the lack of significant historical tsunami events in the GoM, the degree of landslide tsunami hazard in the GoM and for U.S. Gulf Coast states is not well understood. Therefore, determining the potential impact of these events on coastal communities depends on detailed geologic analysis/source characterization and reliable numerical landslide tsunami models to determine tsunami generation behavior and inundation threat. One of the main challenges to accurate and efficient submarine landslide tsunami modeling is source determination. Three large-scale ancient maximum credible submarine landslides with tsunamigenic potential have been recognized [*ten Brink et al.*, 2009a] which represent possible worst-case tsunami scenarios affecting GoM coasts in the past. However, these events occurred over 7000 years ago and are widely spaced along the GoM continental shelf. Without more data on recent events to help characterize tsunamigenic SMF activity within the GoM, a deterministic approach to mapping regions of increased landslide tsunami hazard potential within the GoM is not possible. It is therefore necessary to develop nondeterministic methods to supplement and fill the gaps between the ancient existing sources in order to more accurately determine risk and regions of enhanced hazard for the GoM. Numerical modeling of submarine landslide tsunami generation is too computationally intensive to allow for a full-scale probabilistic assessment involving multiple SMF scenarios across the entire GoM. Therefore, as a first-order estimate of tsunamigenic potential, a Monte Carlo Simulation (MCS) methodology is implemented to determine trial SMF scenarios and calculate the probability of failure and tsunami generation. Previous studies by *Maretzki et al.* [2007] and *Grilli et al.* [2009] used a similar MCS approach to assess landslide tsunami hazard along the east coast of the United States, and work by *Shigihara and Horrillo* [2014] applied the techniques of *Maretzki et al.* [2007] and *Grilli et al.* [2009] to the unique bathymetry of the GoM. However, while those studies determined potential slope failure based on independent distributions of parameters for landslide location and geometry, strong correlations between certain size parameters are evident based on previous GoM SMF events, specifically the values for area, volume, and length. These correlations suggest a unique importance of these variables to overall SMF behavior. Therefore, the MCS approach discussed here includes a matrix correlation method for these critical submarine landslide parameters based on the Cholesky decomposition method, which enables us to capture both the uncertainty in the parameter values as well as the natural correlations seen in observational SMF data. We assess SMF potential along four transects drawn across the GoM continental slope based on these correlated distributions. Once a trial landslide location/depth and geometry is determined, its probability of failing and producing a tsunami is calculated based on the sediment parameters and seismic loading for that region. The annual probability of these events is determined by the joint probability of slope failure with the annual probability of the triggering earthquake. Those SMF scenarios which produce the largest tsunami amplitude and have the highest probability (shortest return period) are deemed the most extreme probabilistic events for each individual transect, and the dimensions of these events are averaged to determine a single Probabilistic Maximum Credible Event (PMCE) for each transect. These PMCEs provide a first-order estimate of tsunami potential and recurrence for the GoM. In a full-scale tsunami hazard assessment, the PMCEs can be used in a more deterministic manner to model full-scale tsunami generation, propagation, and inundation of coastal cities with an idea of likelihood of occurrence.

This paper is organized as follows. Section 2 gives an overview of the methodology used in our MCS approach, with section 2.2 describing the matrix correlation method for landslide parameters. Section 3 discusses the statistical relevance of the method and the resulting SMF scenarios calculated for each transect. Section 4 gives concluding remarks and suggestions for improvements to this work.
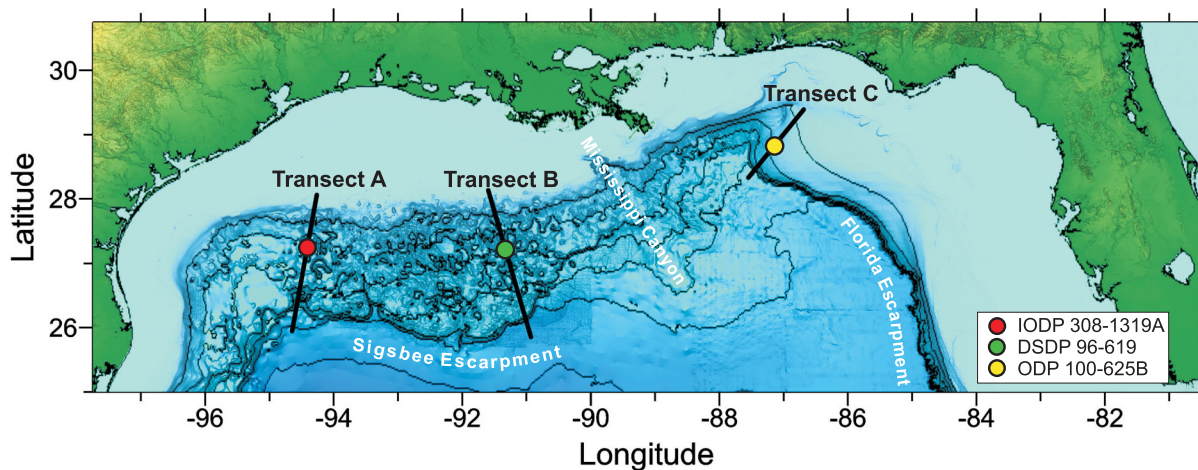
Figure 1. Locations of GoM sediment data used from the IODP (red circle), DSDP (green circle), and ODP (yellow circle) drilling surveys and transects (black lines) used in this study. Bathymetry contours are at 500 m levels. Bathymetric features are indicated for reference.

2. Methodology

The MCS methodology discussed here to determine SMF sources expands on that presented in *Maretzki et al*. [2007], *Grilli et al*. [2009], and *Shigihara and Horrillo* [2014], and a summary of the procedure is as follows. An MCS routine is employed to determine the size and location of trial SMFs along a given transect across the continental slope of the GoM based on distributions for landslide parameters as determined from observational data [*McAdoo et al*., 2000; *ten Brink et al*., 2009a]. For each trial landslide, the factor of safety for slope stability is calculated based on the location and size of the landslide, sediment properties, and the local peak horizontal ground acceleration (PHA) to determine if it will fail and possibly produce a tsunami. For those configurations that fail, an initial tsunami amplitude is estimated, and, if the tsunami amplitude is above a certain minimum threshold amplitude, that SMF is considered tsunamigenic. The probability of a tsunamigenic SMF is determined as the joint probability of the earthquake occurrence and the probability of slope failure.

2.1. Geophysical and Landslide Data

The current study focuses on landslide tsunami hazard from sources within the northern GoM (see Figure 1). Expanding documentation on the occurrence of landslides along the Campeche margin, e.g., from *Chaytor et al*. [2014], will allow for future assessment of tsunami events originating in the southern part of the GoM, though the contribution of such events is excluded for now. The northern GoM features a very wide continental shelf throughout, relatively mild slopes, and bathymetry that varies considerably from west to east in three distinct geologic provinces: a salt province to the west-northwest, a deep-sea fan province in the north and central part of the basin, and a carbonate province to the east-northeast. Bathymetry tends to smooth out from west to east. In the west-northwest salt province, overlying sediments are moved by salt formation movement across the continental slope, leading to numerous small basins and very rough and uneven bathymetry. In the northern part of the GoM, thick sediments are provided by the Mississippi River, leading to the fan province which spreads from the Mississippi Canyon into the central GoM basin. The carbonate province, which follows the western coastline of Florida, features a progression of carbonate sediments from north to south, with thicker carbonate sediments to the south. The bathymetry along the eastern continental slope is very regular and smooth in comparison to that of the northern and northwestern slope.

According to a survey of submarine landslides along U.S. coastal regions by *McAdoo et al*. [2000], the GoM contains the largest (in both area and volume) SMF footprints across all U.S. continental margins, and the GoM also features the widest range in magnitude of SMF area. The largest slides occur near the Mississippi Canyon in bathymetrically low regions of the deep-sea fan province, while the smallest failures are found within the salt provinces [*ten Brink et al*., 2009a; *McAdoo et al*., 2000]. This suggests that landslide behavior is
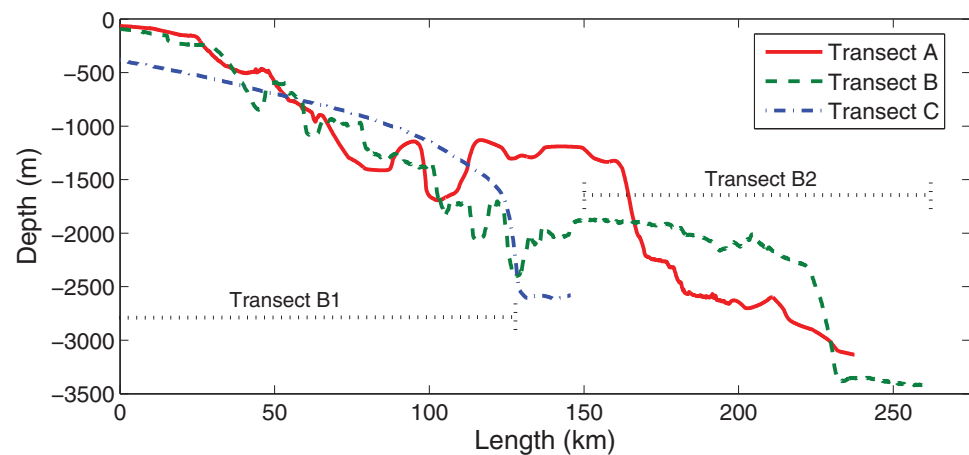
Figure 2. Bathymetry profiles for Transects A (solid), B (dashed), and C (dot-dashed) across the GoM continental slope. Dotted black lines show extents of Transects B1 and B2 split from Transect B.

therefore partially a function of geologic processes, which are manifested in the bathymetry by regions of different bathymetric smoothness/regularity and slope.

Information on sediment properties for the GoM comes from publicly available data of the Deep Sea Drilling Project (DSDP, 1966–1983), Ocean Drilling Program (ODP, 1985–2003), and Integrated Ocean Drilling Program (IODP, 2003–2013). Locations where deep (>100 m below the seafloor) sediment data exist are used to construct transects across the GoM continental slope. Specifically, in this study, sediment data are obtained from IODP Leg 308 Site 1319A in the northwest GoM, DSDP Leg 96 Site 619 in the north central GoM, and ODP Leg 100 Site 625B in the northeast. We consider three transects drawn across the GoM continental slope through these drilling sites. These transects and the locations of the drilling sites are shown in Figure 1. Transects are labeled as Transect A through site IODP 308-1319A, Transect B through site DSDP 96-619, and Transect C through site ODP 100-625B. The bathymetry profile along each of these transects is shown in Figure 2. Transects A and B exhibit very irregular bathymetry due to movement of salt and overlying sediments in this province. However, it is noticeable that the first approximately 120 km of Transect B is highly irregular, while from approximately 150 km on the transect displays a smoother, more regular profile with a very clear slope increase defining the Sigsbee Escarpment. While these two regions are both part of the salt province and are not significantly geologically different, due to the clear geomorphological differences seen between the sections and the differences in submarine landslide size seen among regions of differing geomorphology [*ten Brink et al.*, 2009a; *McAdoo et al.*, 2000], it is reasonable to expect these two sections of Transect B to show different behavior in terms of landslide potential. Therefore, for the purposes of this study, Transect B is subsequently partitioned into two sections: Transect B1 from the beginning to roughly 120 km and Transect B2 from approximately 150 km to the end of the transect. Transect C lies across the northern part of the West Florida Slope carbonate platform and clearly exhibits very smooth and regular bathymetry with the well-defined steep slope of the Florida Escarpment.

The data from the drilling sites have been used to determine sediment properties, specifically density and undrained shear strength, along each transect. Discrete data from each site are used to determine curves for the bulk density ρ_S and undrained shear strength su as functions of depth below the seafloor. The bulk density and undrained shear strength for the transects considered here are shown in Figure 3. Note that the sediment properties for Transect B are assumed applicable to both Transect B1 and Transect B2. While it is expected that sediment properties vary along each transect, due to the limitation of sediment data at the drilling site locations and not along the transects, it is assumed that the data from each drilling site is valid along the entirety of its intersecting transect. This seems to be a reasonable estimate given the first-order, engineering-based model of slope stability used here (discussed later) which depends on single values for sediment parameters, as well as uniform values for landslide dimension/slope across the failure region.

Seismic data obtained from the U.S. Geological Survey (http://earthquake.usgs.gov/hazards/products/conterminous/2014/data/) are used to determine a map of PHA, given as a fraction of the gravitational
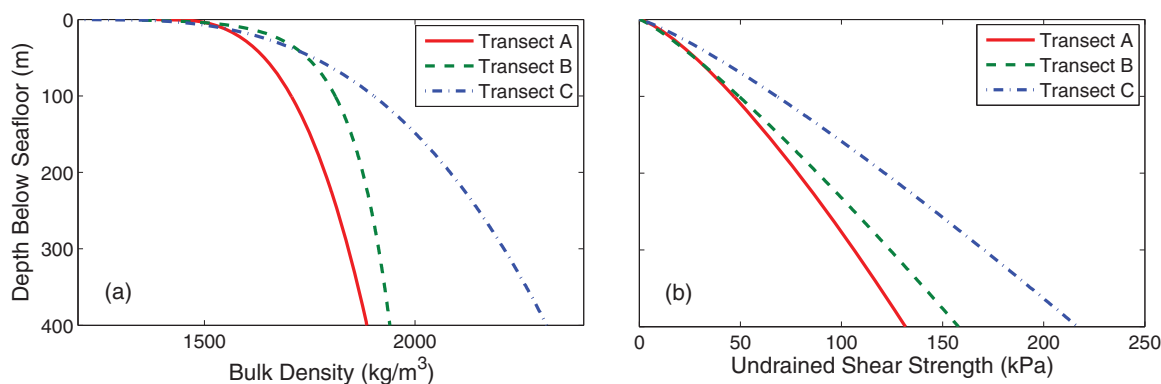
Figure 3. (a) Bulk density and (b) undrained shear strength for Transects A (solid), B (dashed), and C (dot-dashed), obtained from sediment data from the offshore drilling programs.

acceleration g, throughout the northern GoM, which is shown in Figure 4 for the specific exceedance probability of 2% in 50 years. The PHA for any location within the northern GoM can be determined from a curve fit of USGS seismicity data for PHA and annual probability of exceedance $P_{PHA} = 1/\lambda$, the inverse of the period of return λ for an earthquake with that PHA. An example of such a hazard curve is shown in Figure 5 for the location 86.7°W, 25.7°N. In this way, given a specific return period, or the annual probability of exceedance, for a certain location, the PHA for that location can be determined. In the MCS model, PHA is calculated for a range of earthquake return periods of 10–10,000 years (P_{PHA} of 0.1–0.0001). Details of the influence of the return period on potential slope failure are discussed further in section 2.3.

2.2. Monte Carlo Simulation: Correlated Random Variables

The MCS method depends on statistical distributions for GoM submarine landslide parameters, obtained from 25 landslides analyzed in *McAdoo et al.* [2000] as well as three additional ancient landslides described in *ten Brink et al.* [2009a]. Within the MCS routine, sets of random values are chosen for depth, area, volume, and length based on their distributions. These parameters are selected as essential based on the necessity of determining a location and size for the trial landslide. Clearly, depth is essential to determine a trial landslide location along the transect. Area, volume, and length are chosen as the critical size parameters based on trends seen in the data discussed below. The cumulative probability distributions for observational values of depth, area, volume, and length are shown in Figure 6. Dashed lines are the reference line for either a normal or lognormal distribution, depending on the parameter, indicating a perfect fit to that distribution type. The probability distribution for depth is normal, while those for area, volume, and length are lognormal. In all cases, the data values follow the respective reference line very well, indicating a clear normal (depth) or lognormal (area, volume, length) distribution.

Randomness is critical to a probabilistic assessment of landslide tsunami hazard because large uncertainty, both epistemic and aleatoric, exists in the size and location of submarine failures. Naturally, the specific size and location of an individual landslide event varies from one event to another. Further uncertainty exists in the distributions determined for each size parameter due to measurement error as well as a limited number of previous events from which to take measurements. The difficulty of sensing and mapping submarine landslides makes smaller failures easier to miss, possibly skewing the data toward larger events. Even in light of these uncertainties, the observational data show that SMF size parameters do not seem to be completely random, but correlations between certain parameters seem to be an important attribute of submarine landslide behavior. In particular, submarine landslide volume and area are very well correlated, as shown by *McAdoo et al.* [2000] for slides off the west, east, and GoM coastal regions of the U.S. and by *ten Brink et al.* [2006] for slides off the north coast of Puerto Rico. Specifically, for the past GoM SMF events used here, volume and area have a strong correlation coefficient of $\rho = 0.9572$ (based on the associated normal distributions of the lognormal volume and area). In addition, length is also evidently well correlated with both volume and area of GoM landslides, as seen in Figure 7. The correlation coefficients for these parameters are $\rho = 0.9331$ for length and area, and $\rho = 0.8698$ for length and volume.
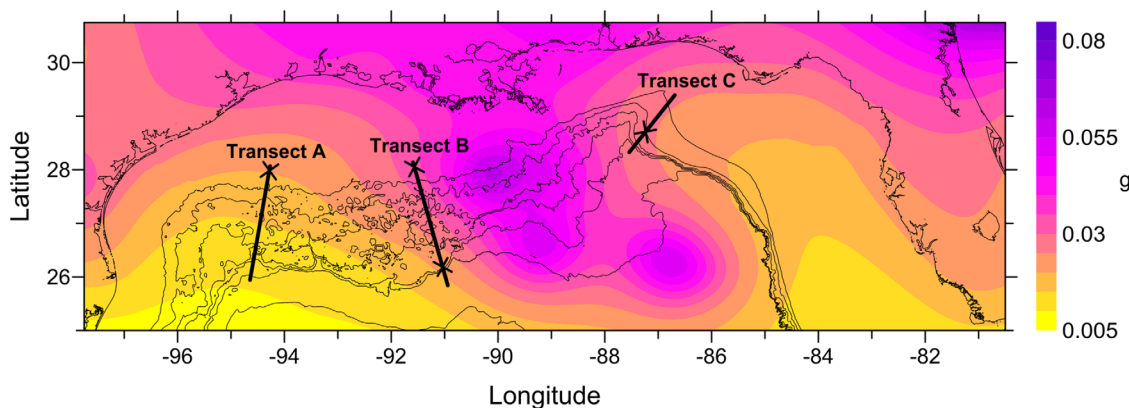
Figure 4. Peak Horizontal Acceleration (PHA, as a fraction of gravitational acceleration g) for a probability of exceedance of 2% in 50 years in the northern GoM. Bathymetry contours are at 500 m levels. Black crosses mark approximate locations of PMCE headscarps determined from the MCS model (see section 3).

These evident mutual correlations prompted us to incorporate these trends in the probabilistic assessment of landslide tsunami hazard in the GoM. In this way, the MCS methodology presented here deviates from that of *Maretzki et al.* [2007], *Grilli et al.* [2009], and *Shigihara and Horrillo* [2014]. In those works, landslide dimensions of volume, length, and thickness are determined as random values drawn independently from their respective distributions. However, this approach does not take into account the obvious relationships seen from the significant correlation coefficients. Here to maintain those relationships within the MCS model, we implement a Cholesky decomposition of the covariance matrix for area, volume, and length, based on the outline given in *Thomopoulos* [2012]. Through this approach, the individual variables still follow their respective independent distributions, yet are allowed to vary based on their mutual correlations.

Since area (A), volume (V), and length (L) follow lognormal distributions, the natural logarithm of these variables are normally distributed. The associated normal distributions for area, volume, and length have means of μ_A, μ_V, and μ_L, respectively. The Cholesky decomposition of the positive definite covariance matrix Σ for the associated multivariate normal distribution is given by

$$\Sigma = CC^T \qquad (1)$$

with C a lower triangular matrix. Then, from a set of random normal variables $u_i \sim N(0, 1)$, correlated normal variables X, Y, and Z can be determined by
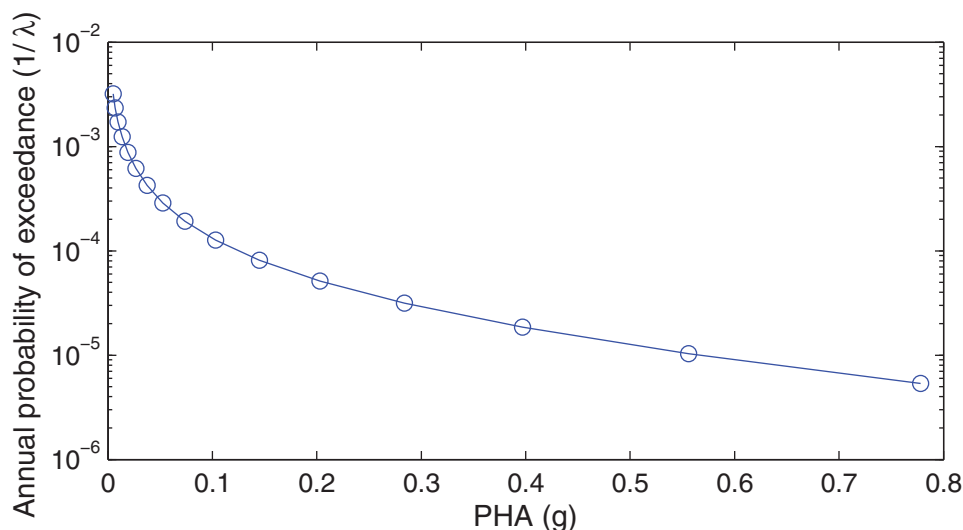

Figure 5. Example hazard curve for annual probability of exceedance $1/\lambda$ versus PHA for the location 86.7°W, 25.7°N.
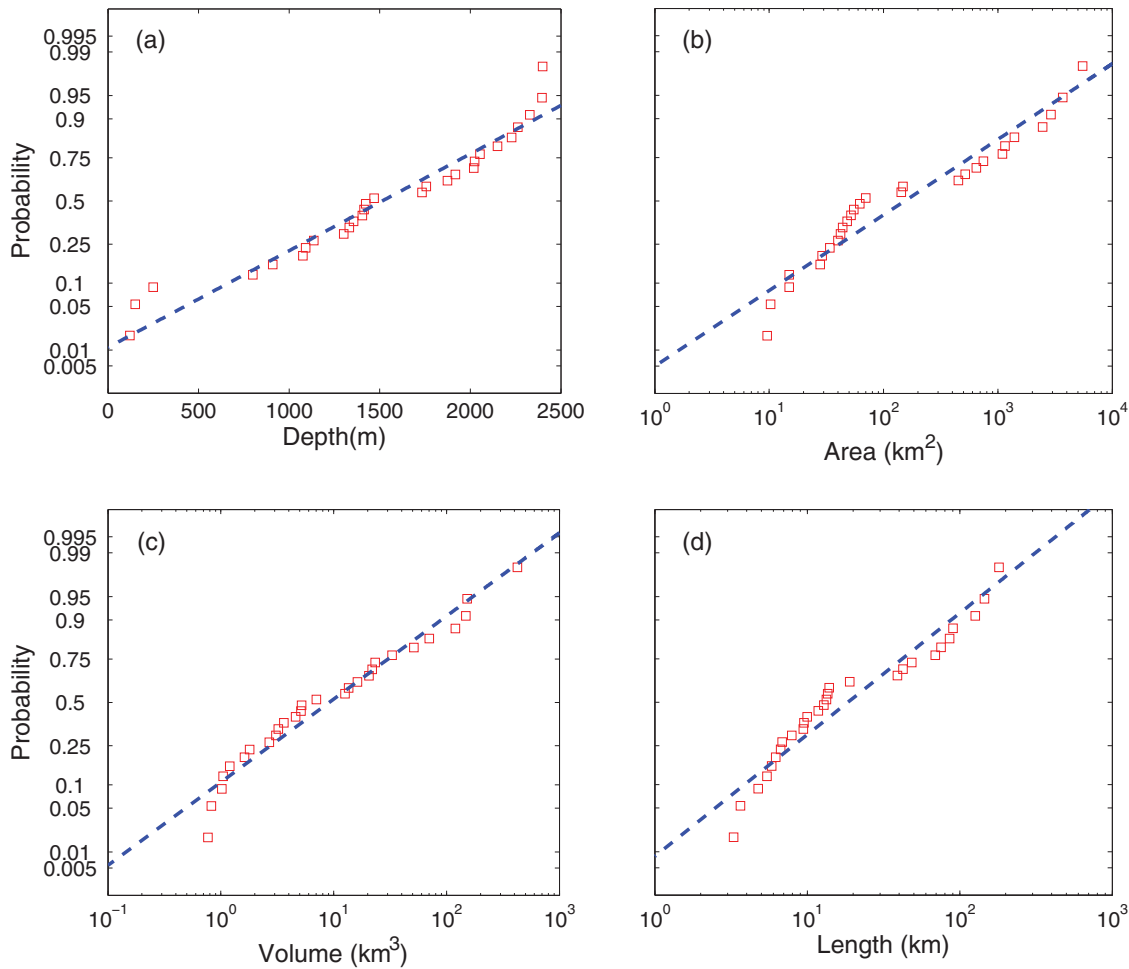
Figure 6. Cumulative probability distributions of GoM observational submarine landslide data for (a) depth (normal distribution), (b) area (lognormal distribution), (c) volume (lognormal distribution), and (d) length (lognormal distribution).

$$\begin{bmatrix} X \\ Y \\ Z \end{bmatrix} = C \begin{bmatrix} u_1 \\ u_2 \\ u_3 \end{bmatrix} + \begin{bmatrix} \mu_A \\ \mu_V \\ \mu_L \end{bmatrix} \tag{2}$$

Then, the correlated lognormal variables A, V, and L are found from

$$\begin{bmatrix} A \\ V \\ L \end{bmatrix} = \exp([X, Y, Z]^T) \tag{3}$$

Width of the landslide is then calculated simply as $W = A/L$. Likewise, landslide thickness (vertical headscarp height) is determined as $T = 2V/A$.

For each set of parameters determined as above, the depth, length, and thickness are used to determine the unfailed seafloor slope and failed slope angles based on the actual transect bathymetry. Data for area and seafloor slope show a general trend in submarine landslide behavior: the smaller the seafloor slope, the larger the landslide area, as shown in Figure 8 for the GoM [*McAdoo et al.*, 2000], and as also noted by *Hühnerbach and Masson* [2004] and *Masson et al.* [2006] for other regions. Therefore, to ensure that the MCS model does not produce a large landslide with an unnaturally large slope, the MCS values for area and seafloor slope are constrained to lie beneath a maximum slope-versus-area envelope, found by creating a fit through the uppermost data values corresponding to maximum slope for a given area (Figure 8, dashed line). In order to avoid a zero-
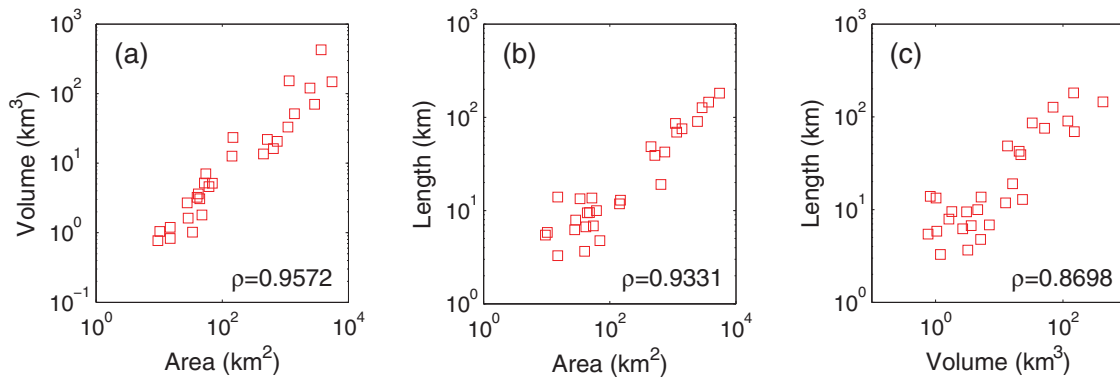
Figure 7. Data correlations from GoM observational submarine landslide data for (a) volume and area, (b) length and area, and (c) length and volume. Correlation coefficients ρ are also shown.

slope situation in applying this maximum envelope, a seafloor slope of 2° is chosen as the limit of the envelope for areas greater than 4697 km^2 (the intersection of the curve fit and the 2° line). If, for a calculated area, the seafloor slope lies above the maximum envelope (or a negative slope is encountered), new values are determined for area, volume, and length via the Cholesky decomposition approach.

2.3. Probability of a Tsunamigenic SMF

Once the landslide dimensions are selected, a slope stability analysis is performed to determine if the trial landslide will fail. The factor of safety of the trial landslide is calculated based on the infinite slope method for translational failures, assuming large-scale slides with $L \gg T$; this method is reasonably valid for the GoM given the observed data and relatively mild slopes. The available sediment data indicate that sediments at the sites considered here are mostly fine-grained cohesive soils consisting of predominantly silty clay, which under dynamic earthquake loading would be expected to exhibit undrained failures [*Morgenstern*, 1967]. Thus, the factor of safety *FS* for a cohesive, translational slide is given considering a total stress analysis relating sediment undrained shear strength *su* to the shear stress τ, which combines the downslope gravity force with a pseudostatic horizontal component for earthquake loading [*Morgenstern*, 1967; *ten Brink et al.*, 2009b]:
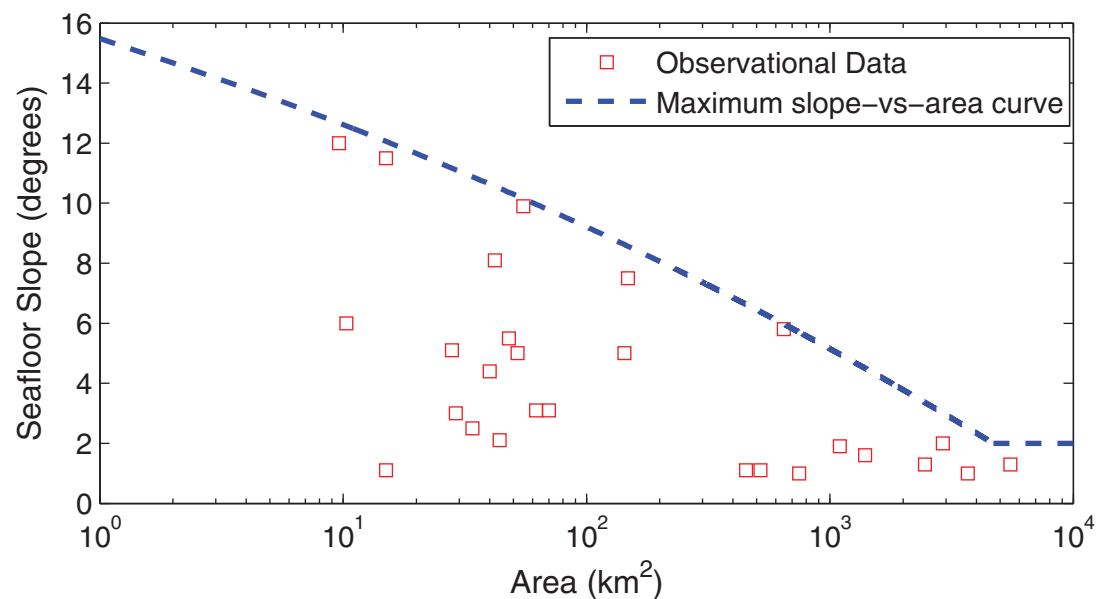

Figure 8. Unfailed seafloor slope versus area for observed GoM submarine landslides. Squares indicate data points. Dashed line represents maximum slope-versus-area envelope allowed in the MCS model, determined by a curve fit through the data points with the maximum slopes for a given area.

$$FS = \frac{su}{\tau} = \frac{su}{Tg[(\rho_S - \rho_W)\sin\beta\cos\beta + k\rho_S\cos^2\beta]} \tag{4}$$

where ρ_S and ρ_W are the densities of the landslide sediment and water, respectively; β is the failed slope angle; k is the seismic coefficient, defined as $k = PHA/g$. A trial landslide is considered a failure event if $FS < 1$, that is, when the shear stress on the slip surface exceeds the shear strength of the sediment.

For those landslides that fail, a maximum tsunami amplitude η is calculated based on a semiempirical formula for maximum tsunami depression above a translational slide determined by *Grilli and Watts* [2005] and *Watts et al.* [2005]:

$$\eta = \frac{\pi V L^{1.25}}{2(A + \lambda_0 L)}(s+1)(0.0574 - 0.0431\sin\beta)\left(\frac{\sin\beta}{D}\right)^{1.25}\left(1 - e^{-2.2(s-1)}\right) \tag{5}$$

where $s = \rho_S/\rho_W$, D is the water depth above the landslide headscarp, and

$$\lambda_0 = \sqrt{\frac{\pi L D (s+1)^2}{2\sin\beta(s-1)}}$$

is the characteristic tsunami wavelength. Note that here it is assumed that the maximum tsunami amplitude follows the same behavior as the maximum tsunami depression. A failure is considered to be tsunamigenic only if the maximum tsunami amplitude η for that event is greater than a certain threshold value η_{th}. Here as in *Grilli et al.* [2009], η_{th} is taken to be 0.02 m or 2 cm. Other threshold values were tested, though it was found that smaller values of η_{th} did not significantly affect the resulting landslide parameter distributions. For some transects, the smaller threshold value resulted in slightly smaller landslide dimensions, though not significantly so, and for the purposes of providing a conservative (overly cautious) estimate of tsunami events, the larger threshold of 2 cm was deemed more appropriate.

Since an SMF is assumed to be triggered by an earthquake in this model, following *Grilli et al.* [2009], the probability of a tsunamigenic SMF, P_{SMF}, is calculated as the joint probability of exceedance of the earthquake, P_{PHA}, with the probability that that earthquake causes a calculated trial landslide to fail and produce a tsunami wave, P_f, so that

$$P_{SMF} = P_{PHA}P_f \tag{6}$$

where

$$P_f = n/N \tag{7}$$

with n the number of tsunamigenic failures for a certain earthquake return period λ and N the total number of trial landslides generated by the MCS model for the transect under analysis. The resulting return period of the tsunamigenic SMF is given by $\lambda_{SMF} = 1/P_{SMF}$. In the MCS routine, the period of return λ is increased incrementally from 10 to 10,000 years for each trial landslide to determine the minimum earthquake return period and PHA (if any) that will cause that configuration to fail based on the calculated FS. By the nature of FS, any larger PHA, and therefore larger return period, will induce a failure as well.

Given the randomness involved in this probabilistic approach, realistic results and model convergence can be expected only with a certain number of MCS trial landslides. As discussed in *Nowak and Collins* [2000] and *Grilli et al.* [2009], the maximum SMF return period $\lambda_{S_{max}}$ that can be accurately estimated from a set of N simulations is given by

$$\lambda_{S_{max}} = \frac{1}{N CoV^2 + 1} \tag{8}$$

where CoV is the coefficient of variation. As in *Grilli et al.* [2009], a $CoV = 0.1$, or 10% is used. Only three of the GoM SMFs used here to form the parameter distributions have been age dated and are estimated to be older than 7500 years. Based on this historical age data, we aim to determine the most frequent tsunamigenic SMFs, or those with a return period up to $\lambda_{S_{max}} = 10,000$ years. Thus, $N = 1,000,000$ trial landslide calculations are performed for each transect in order to ensure realistic MCS results and model convergence.

2.4. Probabilistic Maximum Credible Event

The Probabilistic Maximum Credible Event (PMCE) for each transect is defined here as the failure that produces the largest maximum tsunami amplitude and that occurs with the highest rate of recurrence or highest probability. Since several different landslide configurations may fail for a given λ, leading to multiple events with the same return period λ_{SMF} but with different tsunami amplitudes, we identify the extreme value of tsunami amplitude, η_{max}, for each λ_{SMF}. The η_{max} event which has the highest rate of recurrence, or shortest return period, will describe the PMCE. The smallest SMF return periods calculated from the joint probability are on the order of thousands of years, so probabilities are small, and negligible change in probability is seen as the return period is varied by a few hundred years. In an effort to determine a single PMCE for each transect, all events with essentially the same probability are considered collectively. Thus, the η_{max} extreme value events with return periods that fall into the first 100 years from the minimum calculated return period for a specific transect are considered representative of the highest-probability SMF event for that transect; this 100 year return period range is termed $\lambda_{S_{100}}$. For example, if the minimum return period for a transect is calculated to be 1000 years, all η_{max} events for that transect with a return period less than or equal to 1100 years are collected as a set of extreme events with probability 0.001. The PMCE for a transect is then determined by calculating mean values for location (depth) and dimension (area, volume, length, width, and thickness) from all of that transect's η_{max} events with a return period in $\lambda_{S_{100}}$.

3. Statistical Analysis and Results

Table 1 details the distributions and the values used in the MCS model, as determined from *McAdoo et al.* [2000] and *ten Brink et al.* [2009a]. The values μ and σ are the mean and standard deviation, respectively, in the case of a normally distributed parameter. In the case of a lognormal distribution, they correspond to the parameters of the distribution, or the mean and standard deviation of the natural logarithm of the distribution. Note that while distributions are indicated for Width and Width/Length, these are for informational purposes only; only the distributions for depth, area, volume, and length are used to determine random landslide location and size parameters within the MCS model. The column "Data Range" in Table 1 indicates the range of values seen in the observational data used here [*McAdoo et al.*, 2000; *ten Brink et al.*, 2009a]. Certain constraints were imposed on the range of some landslide dimensions in the MCS model in order to maintain physically relevant trial landslides. These constraints are given in the "MCS Constraints" column. The range of depths allowed in the MCS model varies across transects depending on the actual bathymetry so that failures can only occur at depths within the depth range of the individual transect. The value of "N/A" for volume indicates that no limitations were set for the volume a trial landslide could have. Values for area, length, and width were allowed to extend outside the range of those seen in the data in order to allow for variability from previous measurements. However, maximum values were restricted to two standard deviations from the mean of the associated normal distributions, corresponding to a cumulative probability of approximately 0.977. This limit was imposed in order to allow landslides larger than those which have been measured, while excluding those which may become unreasonably large with respect to the size of the GoM itself. Length was additionally constrained for each transect in that the landslide length from the headscarp location cannot go beyond the end of the transect. The constraints for width/length were taken approximately from the data range in order to prevent unnaturally long and narrow failures and, likewise, those which are excessively wide.

Figure 9 shows cumulative probability distributions of typical tsunamigenic ($\eta \geq \eta_{th}$) MCS model results for depth, area, volume, and length—those parameters which are randomly selected from their distributions in the model. For brevity, only the distributions for Transect C are shown. Results for the other transects are comparable. Once again, the dashed line is the reference line for the normal or lognormal distribution. It is clear that the MCS model results exhibit the expected normal (depth) or lognormal (area, volume, length) distributions. Deviations from the reference line occur where the MCS values are restricted as discussed above. The distribution for depth shows the most deviation due to the constraints imposed by the transect bathymetry. Distributions for additional parameters, such as thickness and width (not shown), were also verified to follow their expected distributions based on the observational data.

Figures 10–13 show volume versus area, length versus area, and length versus volume for tsunamigenic failures calculated by the MCS model (blue circles) as compared to observational data (red squares, same as in

Table 1. MCS Input Values for Landslide Location and Dimension[a]

Parameter	Distribution	μ	σ	Data Range	MCS Constraints
Depth (m)	Normal	1513.32	661.76	121–2399	Varies
Area (km^2)	Lognormal	5.03	1.95	9.6–5509	0–7659.5
Volume (km^3)	Lognormal	2.21	1.78	0.8–425	N/A
Length (km)	Lognormal	2.92	1.22	3.28–180.91	0–210.73
Width (km)	Lognormal	2.12	0.928	1.078–34.1	0–53.28
Width/Length	Lognormal	−0.796	0.932	0.07747–3.09	0.07–2.9

[a]Distributions and range of values used for landslide location and size in the MCS model. Parameters μ and σ are the mean and standard deviation, respectively, in the case of a normal distribution, while for a lognormal distribution, they correspond to the parameters of the distribution, i.e., the mean and standard deviation of the logarithm of the distribution.

Figure 7). Overall, sizes of tsunamigenic failures generated by the MCS routine are consistent across the transects, although smaller SMFs are possible in Transect C as compared with the others. We find that implementing the Cholesky decomposition approach for random correlated variables within the MCS model results in values that encompass the historical data very well while still exhibiting variability that would be expected in nature. In cases where the observational data lie outside the model results, the MCS results are restricted due to either the constraints imposed within the MCS model as discussed above or to the limitation that the maximum return period of 10,000 years that can be accurately estimated by the MCS model; any configurations which result in a return period greater than 10,000 years are excluded. Additionally, since data for previous SMF events were combined to determine the governing distributions, not considering local bathymetric influences, the large observed slides which lie outside of the MCS model results for a given transect may be physically unrealistic for that region due to the local bathymetry.

The η_{max} extreme value events which initiate the maximum tsunami amplitudes are indicated by yellow dots in Figures 10–13. The set of η_{max} events with return periods in $\lambda_{S_{100}}$ (the most likely extreme events) is indicated by black stars. Table 2 shows the range of minimum return periods $\lambda_{S_{100}}$ as well as the range of earthquake return periods λ required to trigger these tsunamigenic failures.

It is interesting to note that the extreme η_{max} events are not necessarily those with the maximum overall dimensions. That is, the yellow dots in Figures 10–13 do not lie exclusively in the upper right portion of the tsunamigenic MCS results. This is due at least in part to the balance of area, volume, and length, as well as depth, terms in (5), since tsunami amplitudes in our model rely on this semiempirical equation. In reality, this is seen when smaller failures occur in shallow water depths, producing relatively large tsunami waves. Additionally, even for deeper, smaller failures or those on steep slopes which would not be expected to produce a large amplitude wave, if the Froude number of the landslide is close to 1, amplification of the wave may occur, resulting in a relatively large-amplitude tsunami. However, different behavior is seen across the transects. For Transects A and B1, SMFs with larger areas or lengths and smaller volumes tend to produce extreme-amplitude tsunamis. The maximum-amplitude events for Transect C do include the absolute maximum dimension SMFs, but also those with larger areas or lengths and smaller volumes. Additionally, length and area seem to be more equally weighted in producing extreme tsunami amplitudes, as the points for the η_{max} events are mostly centrally located in the length-versus-area plots for Transects A, B1, and C. These results suggest that an SMF with large length and area may be more efficient at producing extreme tsunami amplitudes than one with large volume and relatively small area and length (thus requiring a large thickness). Analysis of results for thickness versus volume and length versus width support this hypothesis as well, as shown in Figure 14 for Transect A. (Similar trends are seen in such plots for Transects B1 and C, so, for brevity, they are not shown here.) A somewhat opposite result seems to be the case for Transect B2. Large volumes tend to govern extreme tsunami amplitudes, even for moderate areas and lengths. Additionally, slides with large area but short length tend to produce extreme tsunami waves for Transect B2.

Furthermore, the most likely extreme events (η_{max} with return period in $\lambda_{S_{100}}$, black stars) do not necessarily correspond to the maximum sizes within the set of extreme amplitude η_{max} events, and there is not a very clear pattern in behavior among the transects. For Transect A, they lie roughly along the line of maximum volume for a given area and occur with larger area or volume for almost any length which resulted in an η_{max} amplitude. The most likely extreme events for Transect B1 occur with larger length and area, but more moderately sized volume. For Transect B2, the extreme events with smallest overall dimensions seem to be
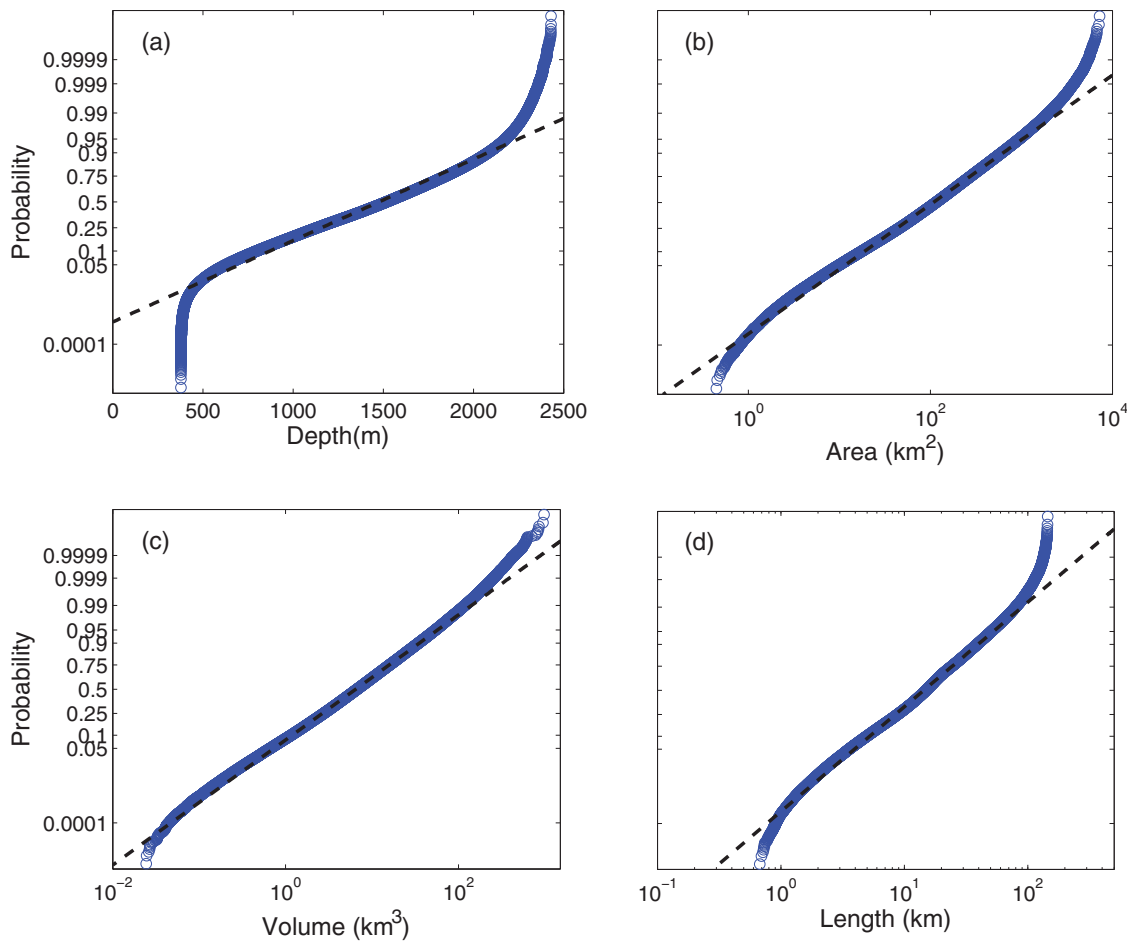
Figure 9. Cumulative probability distributions of tsunamigenic MCS results for the randomly generated parameters: (a) depth (normal distribution), (b) area (lognormal distribution), (c) volume (lognormal distribution), and (d) length (lognormal distribution). For brevity, results are only shown for Transect C. Results for other transects are similar.

the most likely, as could logically be expected. The most likely extreme events for Transect C tend to have larger volume but smaller length and area.

The locations of the calculated slide headscarps determined by the mean PMCE depth for each transect are shown in Figure 4 by black crosses, and the mean dimensions describing the PMCEs for each transect are given in Table 2. The SMFs for Transects A and B1 occur near the shelf break, where the bathymetry profile is
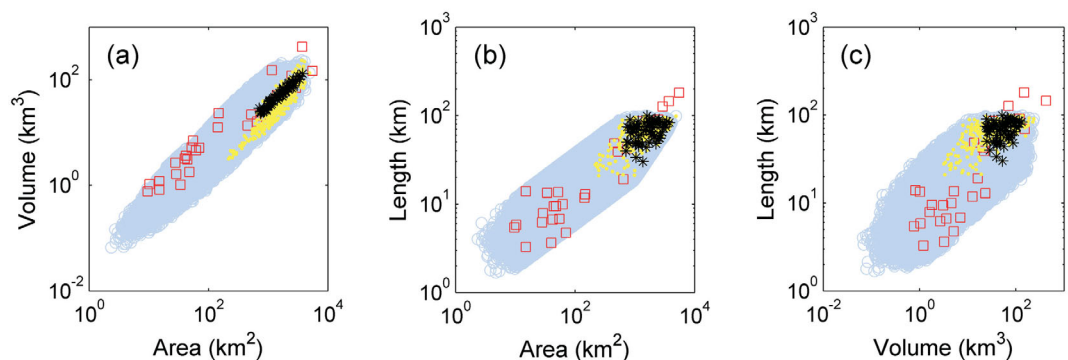

Figure 10. MCS parameter results for Transect A for (a) volume versus area, (b) length versus area, and (c) length versus volume. Blue circles are the tsunamigenic MCS model results ($\eta \geq 0.02$ m). Red squares are observational data (same as in Figure 7). Yellow dots correspond to the extreme tsunami amplitude η_{max} events. Black stars indicate the subset of extreme events with return periods in the first 100 years $\lambda_{S_{100}}$.
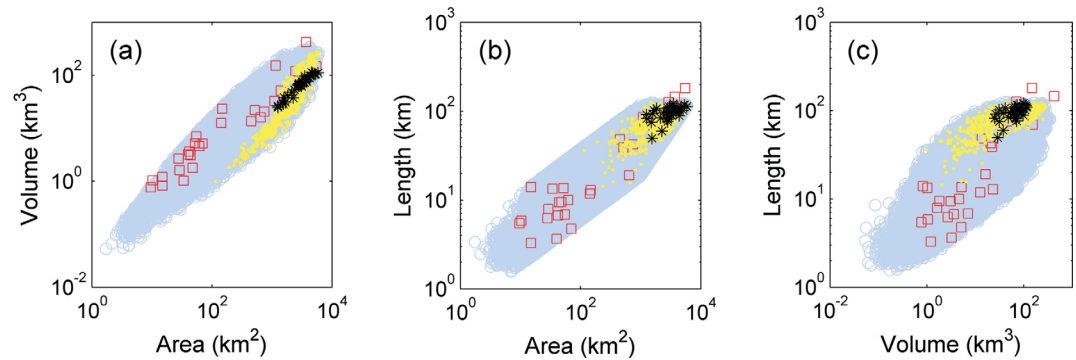
Figure 11. MCS parameter results for Transect B1 for (a) volume versus area, (b) length versus area, and (c) length versus volume. Blue circles are the tsunamigenic MCS model results ($\eta \geq 0.02$). Red squares are observational data (same as in Figure 7). Yellow dots correspond to the extreme tsunami amplitude η_{max} events. Black stars indicate the subset of extreme events with return periods in the first 100 years $\lambda_{S_{100}}$.

smoothest, while for Transects B2 and C they across the Sigsbee and Florida Escarpments, respectively, where the seafloor slopes are steepest. In general, we find that Transects A and B1 exhibit long, narrow ($L/W \approx 3$), and thin PMCEs. Across the steep escarpments, PMCEs for Transects B2 and C are more than 5 times thicker, though shorter by the same order but with comparable widths, leading to more square slides for Transects B2 and C ($L/W \approx 0.6$–0.7). While the PMCEs for Transects A and B1 are significantly smaller in volume and thickness than that for Transect C, they still exhibit the largest mean tsunami amplitudes because of their significantly shallower depths. As could be expected, shallower landslides produce larger initial tsunami amplitudes based on the empirical formulation used here. It is worth noting, however, that these calculations assume the same bathymetry normal to the transect profile. This is more or less accurate for Transects B2 and C which exhibit smooth bathymetry in the normal direction, though clearly an approximation for Transects A and B1.

Return periods of the PMCEs generally range from 5000 to 8000 years ($P_{SMF} \approx 0.000125$–0.0002), though Transect C return periods are an order of magnitude smaller at 550–650 years ($P_{SMF} \approx 0.002$). The minimum return period of the triggering earthquake varies for each transect. Transects A and B1 require a minimum 3500–4500 year return period earthquake ($P_{PHA} \approx 0.00022$–0.0003) to trigger a PMCE. The probability of failure for these transects is comparable at $P_f \approx 0.5$–0.6 for Transect A and $P_f \approx 0.6$–0.7 for Transect B1. These probabilities indicate a fairly good chance of tsunamigenic failure under the seismic loading of a roughly 4000 year earthquake. On the other hand, the MCS method applied to Transect B2 results in a smaller earthquake recurrence period of approximately 350 years ($P_{PHA} \approx 0.003$) required to produce an SMF with a comparable approximately 5000 year return period. This transect has relatively low probabilities of failure ($P_f \approx 0.07$), thus the higher SMF return period compared to that of the triggering earthquake. This suggests that, in this region, conditions must be just right to support a slide failure, even though a large PHA is not necessary.
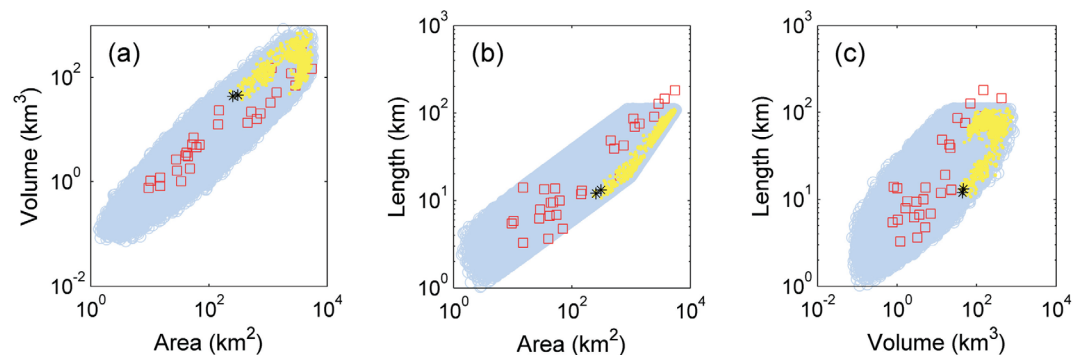

Figure 12. MCS parameter results for Transect B2 for (a) volume versus area, (b) length versus area, and (c) length versus volume. Blue circles are the tsunamigenic MCS model results ($\eta \geq 0.02$). Red squares are observational data (same as in Figure 7). Yellow dots correspond to the extreme tsunami amplitude η_{max} events. Black stars indicate the subset of extreme events with return periods in the first 100 years $\lambda_{S_{100}}$.
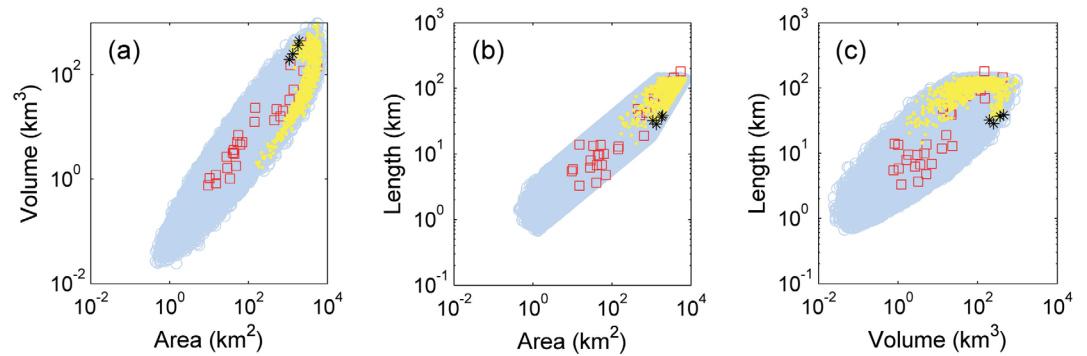
Figure 13. MCS parameter results for Transect C for (a) volume versus area, (b) length versus area, and (c) length versus volume. Blue circles are the tsunamigenic MCS model results ($\eta \geq 0.02$). Red squares are observational data (same as in Figure 7). Yellow dots correspond to the extreme tsunami amplitude η_{max} events. Black stars indicate the subset of extreme events with return periods in the first 100 years $\lambda_{S_{100}}$.

Given the limited data on recurrence intervals of submarine landslides (particularly those that may be tsunamigenic) in the GoM, it is difficult to assess the level of uncertainty in the return periods calculated by the MCS methodology presented here. Since return periods of tsunamigenic SMFs are calculated directly from the PHA and failure probabilities, whatever uncertainty exists in the seismic data is directly translated to the SMF return period. The number of trial landslides calculated is determined to ensure MCS model convergence (with a given coefficient of variation of 10%), so it is assumed that probabilities of failure are represented as accurately as can be expected from a randomized process. Some general observations on the accuracy/validity of the calculated return periods can be made though. The return periods of PMCEs for Transects A, B1, and B2 are slightly lower than the ages of the East Breaks (10,000–25,000 years), Mississippi Canyon (7,500–11,000 years), and West Florida (>10,000 years) landslides as given by *ten Brink et al*. [2009a]. However, the overall mean return period of tsunamigenic failures across these three transects is 7745 years, which falls within the age range of the Mississippi Canyon landslide. Additionally, the return periods of the PMCEs for Transects A, B1, and B2 are in good agreement with mean return times of 6000–8000 years calculated by *Geist et al*. [2013] for a set of submarine mass deposits in the Ursa Basin near the Mississippi Canyon.

The results for Transect C of only 550–650 years between occurrences are significantly smaller than the other transects. The earthquake return periods required to produce failures for this transect are 130–160 years ($P_{PHA} \approx 0.006$–0.008), which is the minimum seen over all of the transects. This combined with moderate probabilities of failure $P_f \approx 0.25$ lead to the observed short SMF return periods. The higher seafloor slopes across the Florida Escarpment where the PMCE for Transect C occurs may contribute to these higher probabilities of failure. The seafloor slopes for tsunamigenic failures along this transect are still notably low at 3.4° on average (compared to 1.5°–2.7° for the other transects), and there is evidence that the number of failures increases with slope for slope angles below ∼5° [*Booth et al*., 1993; *Hühnerbach and Masson*, 2004; *Masson et al*., 2006].

Table 2. Probabilistic Maximum Credible Submarine Landslide Tsunami Events[a]

Transect	A	B1	B2	C
Number of events	64	34	2	4
$\lambda_{S_{100}}$ (years)	7700–7800	5400–5500	4700–4800	550–650
λ (years)	3940–4570	3460–3790	340–350	130–160
Depth (m)	85	130	2323	1098
Area (km^2)	1686	3118	282	1529
Volume (km^3)	57	69	45	315
Length (km)	68	96	13	34
Width (km)	25	32	22	46
Thickness (m)	67	44	323	404
η (m)	61	36	3.0	19

[a]Return period range $\lambda_{S_{100}}$ is the first 100 years of return periods for tsunamigenic SMFs generated by the MCS method, and λ is the corresponding return period range of the triggering earthquake. Single values of landslide depth and size parameters and maximum tsunami amplitude η are those for the PMCE, calculated as the mean values across all extreme-amplitude (η_{max}) tsunami events with return periods in $\lambda_{S_{100}}$.
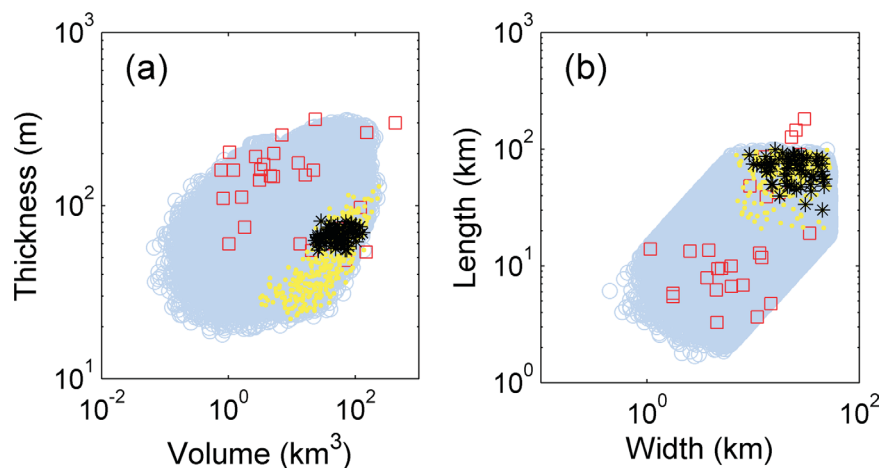
Figure 14. MCS parameter results for Transect A for (a) thickness versus volume and (b) length versus width. Blue circles are the tsunamigenic MCS model results ($\eta \geq 0.02$ m). Red squares are observational data (same as in Figure 7). Yellow dots correspond to the extreme tsunami amplitude η_{max} events. Black stars indicate the subset of extreme events with return periods in the first 100 years $\lambda_{S_{100}}$.

Additionally, overall mean sizes of tsunamigenic failures for this transect are slightly smaller than for the other transects, in agreement with the expectation that smaller failures are more frequent. Enhanced seismic loading in this region can also partially support this result: a study of PHA for an earthquake with recurrence of once in 145 years, based on a map similar to that in Figure 4, indicates that PHA levels in the vicinity of Transect C (approximately 0.0055 g) are higher than along the other transects (0–0.004 g). Additionally, the undrained shear strength and bulk density for Transect C—at depths around the mean thickness of 404 m below the seafloor—are smaller than those of the other transects studied here (see Figure 3). This suggests weaker sediment layers and thus smaller seismic loading required to induce tsunamigenic failures. However, it should be noted that the mean thickness generated by the MCS routine is outside the maximum soil depth (235 m) of the sediment data from the drilling site used for Transect C by a factor of almost 2, and there is considerable variability in the data for undrained shear strength at depths greater than approximately 80 m below the seafloor at this site. The sediment cores used for Transects A and B1 extend to depths which far exceed the thicknesses computed here, and there is not significant variability in undrained shear strength for depths encompassing the mean thicknesses. The mean thickness for Transect B2 also exceeds the maximum depth for the sediment data at the drilling location for that transect by a factor almost 2, but the undrained shear strength is more regular relative to Transect C, and the return period for this transect falls within a reasonable range based on Transects A and B1. Limiting the thickness calculated in the MCS routine to the maximum seen in the observed landslide data or to the maximum depth for which sediment data exist does not change the PMCE return period range for Transect C, though calculated slide dimensions are obviously smaller and therefore would be expected to occur more frequently. Thus, we assume that some uncertainty possibly exists in the sediment properties used for Transect C and the calculated return period of an order of magnitude smaller than the other transects should be viewed with some caution.

4. Conclusions

A Monte Carlo Simulation method was implemented based on historical data within the GoM to determine size and location parameters for potential SMFs. The methodology presented here utilized a Cholesky decomposition approach for statistical correlations seen in observational landslide data to allow for more statistically relevant results of MCS-generated landslide parameters. Once trial landslide configurations were generated, the factor of safety was calculated based on landslide size, location, and PHA of the triggering earthquake. Those configurations which failed and produced initial tsunami amplitudes above a threshold value were considered tsunamigenic SMFs. For each transect, those failures which produced the maximum tsunami amplitudes and occurred over a range of the shortest SMF return periods were collected and the values for size and location of these extreme events were averaged to determine a single Probabilistic Maximum Credible Event for each transect.

Implementing the statistical correlations for area, volume, and length within the MCS routine led to landslide parameters which followed the historical data well and exhibited the observed distributions and correlations. We conclude therefore that our approach leads to more statistically relevant results than had we determined each parameter independently from its respective distribution.

Based on the methodology presented here, in general, return periods of 5000–8000 years can be expected for a PMCE within the northern/northwestern GoM in response to a 3500–4500 year earthquake for the upper northern continental slope or a 350 year earthquake across the Sigsbee Escarpment. Transect C, in the northeastern GoM across the Florida Escarpment, produced a PMCE with a much higher return rate of approximately 500–600 years following a 160 year earthquake. It is possible, however, that uncertainty in the sediment data led to more frequent events in the simulations for this transect. The return periods for PMCEs for Transects A, B1, and B2 are in good agreement with mean return times of 6000–8000 years calculated by *Geist et al.* [2013] for a set of submarine mass deposits in the Ursa Basin near the Mississippi Canyon, and the overall mean of return periods for tsunamigenic failures across these three transects is within the age range of the Mississippi Canyon landslide. Based on the good agreement between the return periods for tsunamigenic SMFs in the north and northwest GoM estimated here by the MCS model and the currently available data on ages and recurrence intervals of GoM submarine landslides, we conclude that, overall, our results are a reasonable first estimate of extreme tsunamigenic SMF return periods for the northern GoM.

Further improvements to the probabilistic model could be made with more submarine landslide data and/or historical tsunami data for the GoM where available, as well as more sediment data. Using one sediment data location for an entire transect is admittedly a rough approximation and introduces uncertainty in the failure probability assessment, but this approach is sufficient for a first-order analysis of hazard probability given the existing constraints on availability of sediment data. A more enhanced analysis of SMF hazard regions could be obtained with additional sediment and geology data at multiple locations along each transect so that a more accurate interpolation of density and undrained shear strength could be made for the entire transect. Improvements in determining slope stability from the factor of safety calculation may also be achieved by incorporating the effect of excess pore pressure, which was neglected here. In addition, while bulk density of the sediment data used here is relatively consistent at a given depth, undrained shear strength can show considerable variability, particularly as depth below the seafloor increases. Preliminary investigations into the effect of including randomness in undrained shear strength values do not indicate significant changes in MCS results, though a more comprehensive quantification of uncertainty in this parameter will be considered in future efforts.

It is evident that regions with different bathymetry exhibit different failure mechanisms and tsunamigenic SMF behavior. Each transect also differs as far as which observed landslide dimensions fall outside the MCS method results given the limits imposed in the model. Furthermore, the largest slides, in both area and volume, mapped in *McAdoo et al.* [2000] are located in regions of smooth bathymetry near the shelf break or in the mildly sloping continental rise at either side of the Mississippi Canyon. Thus, it may be more reasonable to partition the observational data and assume different distributions for different regions of the GoM depending on the regularity or irregularity of the local bathymetry, e.g., one set of distributions covering the salt formation region and one for the rest of the GoM. However, the success of this approach would depend on additional observational SMF data that more fully covers the entire spectrum of GoM bathymetric features. Recent, improved high-resolution bathymetry surveys across the GoM will be substantially helpful in this effort, and many improvements to this assessment can be expected as landslide characterizations from this new data become publicly available.

Notation

ρ_S bulk density of sediment (kg m^{-3}).
su   undrained shear strength of sediment (Pa).
g gravitational acceleration (m s^{-2}).
PHA   peak horizontal ground acceleration (in fraction of g).
λ earthquake return period (years).
P_{PHA} annual probability of exceedance of an earthquake with a given PHA.
ρ correlation coefficient.

A	area of landslide (km^2).
V	volume of landslide (km^3).
L	length of landslide (km).
μ_A	mean of normal distribution for log(A).
μ_V	mean of normal distribution for log(V).
μ_L	mean of normal distribution for log(L).
Σ	covariance matrix.
C	lower-triangular Cholesky decomposition matrix.
u_i	random normal variables.
X	normal correlated random variable for area, $X = \log(A)$.
Y	normal correlated random variable for volume, $Y = \log(V)$.
Z	normal correlated random variable for length, $Z = \log(L)$.
W	width of landslide (km).
T	thickness (vertical headscarp height) of landslide (m).
FS	factor of safety for slope stability.
τ	shear stress (Pa).
ρ_W	density of water (kg m^{-3}).
β	failed slope angle (°).
k	seismic coefficient, defined as PHA/g.
η	maximum tsunami depression or amplitude (m).
s	ratio of sediment density to water density.
D	water depth above landslide headscarp (m).
λ_0	characteristic tsunami wavelength (m).
η_{th}	maximum tsunami amplitude threshold, below which a wave is assumed to not be a tsunami (m).
P_{SMF}	annual probability of tsunamigenic SMF.
P_f	probability of failure for a slope configuration.
n	number of tsunamigenic failures for a certain earthquake return period.
N	total number of trial SMF configurations generated by the MCS routine for a transect.
λ_{SMF}	return period of tsunamigenic SMF (years).
$\lambda_{S_{max}}$	maximum SMF return period that can be accurately estimated from N simulations in a MCS routine.
CoV	coefficient of variation.
η_{max}	extreme tsunami amplitude (m).
$\lambda_{S_{100}}$	range of the first 100 years of SMF return periods for events generated by the MCS routine (years).
μ	mean of normal distribution.
σ	standard deviation of normal distribution.

References

Booth, J. S., D. W. O'Leary, P. Popenoe, and W. W. Danforth (1993), U.S. Atlantic continental slope landslides: Their distribution, general attributes, and implications, in *Selected Studies in the U.S. Exclusive Economic Zone*, edited by W. C. Schwab, H. J. Lee, and D. C. Twichell, *U.S. Geol. Surv. Bull.*, *2002*, 14–22.

Brown, D. L. (1964), Tsunami activity accompanying the Alaska earthquake of 27 March 1964, technical report, U.S. Army Eng. Dist., U.S. Army Corps of Eng., Anchorage, Alaska.

Chaytor, J. D., E. L. Geist, C. K. Paull, D. W. Caress, R. Gwiazda, J. U. Fucugauchi, and M. Rebolledo-Vieyra (2014), Preliminary source characterization and tsunami modeling of submarine landslides along the Yucatan Shelf/Campeche escarpment, southern Gulf of Mexico, Abstract OS33B-1063 presented at 2014 Fall Meeting, AGU, San Francisco, Calif.

Cranford, G. (2000), *Tidal Wave, A List of Victims and Survivors, Newfoundland, 1929*, 264 pp., Flanker Press, St. Johns, Newfoundland, Canada.

Dellinger, J. A., and J. A. Blum (2009), Insights into the mechanism of the northern Gulf of Mexico ms 5.3 "Green Canyon event" of 10 February 2006, *Eos Trans. AGU*, *90*(52), Fall Meet. Suppl., Abstracts S53A-1484.

Dugan, B., and J. Stigall (2010), Origin of overpressure and slope failure in the Ursa region, northern Gulf of Mexico, in *Submarine Mass Movements and Their Consequences*, edited by D. C. Mosher et al., pp. 167–178, Springer, Netherlands.

Dunbar, P. K., and C. S. Weaver (2008), U.S. states and territories national tsunami hazard assessment: Historical record and sources for waves, U.S. Department of Commerce, Nat. Ocean. Atmos. Admin., National Geophysical Data Center technical report No. 3.

Fritz, H. M., F. Mohammed, and J. Yoo (2009), Lituya Bay landslide impact generated mega-tsunami 50th anniversary, *Pure Appl. Geophys.*, *166*, 153–175.

Geist, E. L., P. L. Lynett, and J. D. Chaytor (2009), Hydrodynamic modeling of tsunamis from the Currituck landslide, *Mar. Geol.*, *264*, 41–52.

Geist, E. L., J. D. Chaytor, T. Parsons, and U. ten Brink (2013), Estimation of submarine mass failure probability from a sequence of deposits with age dates, *Geosphere*, *9*(2), 287–298.

Grilli, S. T., and P. Watts (1999), Modeling of waves generated by a moving submerged body. applications to underwater landslides, *Eng. Anal. Boundary Elements*, *23*, 645–656.

Grilli, S. T., and P. Watts (2005), Tsunami generation by submarine mass failure. I: Modeling, experimental validation, and sensitivity analysis, *J. Waterw. Port Coastal Ocean Eng.*, *131*, 283–297.

Grilli, S. T., O.-D. S. Taylor, C. D. P. Baxter, and S. Maretzki (2009), A probabilistic approach for determining submarine landslide tsunami hazard along the upper east coast of the United States, *Mar. Geol.*, *264*, 74–97.

Hampton, M., and J. Locat (1996), Submarine landslides, *Rev. Geophys.*, *34*, 33–59.

Harbitz, C. B., F. Løvholt, and H. Bungum (2014), Submarine landslide tsunamis: How extreme and how likely?, *Nat. Hazards*, *72*(3), 1341–1374.

Hornbach, M. J., S. A. Mondziel, N. R. Grindlay, C. Frohlich, and P. Mann (2008), Did a submarine slide trigger the 1918 Puerto Rico tsunami?, *Sci. Tsunami Hazards*, *27*, 22–31.

Horrillo, J., A. Wood, G.-B. Kim, and A. Parambath (2013), A simplified 3-D Navier-Stokes numerical model for landslide-tsunami: Application to the Gulf of Mexico, *J. Geophys. Res. Oceans*, *118*, 6934–6950, doi:10.1002/2012JC008689.

Hühnerbach, V., and D. G. Masson (2004), Landslides in the North Atlantic and its adjacent seas: An analysis of their morphology, setting and behaviour, *Mar. Geol.*, *213*, 343–362.

Knight, W. (2006), Model predictions of Gulf and Southern Atlantic Coast tsunami impacts from a distribution of sources, *Sci. Tsunami Hazards*, *24*, 304–312.

Liu, P. L.-F., T.-R. Wu, F. Raichlen, C. E. Synolakis, and J. C. Borrero (2005), Runup and rundown generated by three-dimensional sliding masses, *J. Fluid Mech.*, *536*, 107–144.

Locat, J., and H. J. Lee (2002), Submarine landslides: Advances and challenges, *Can. Geotech. J.*, *39*, 193–212.

López-Venegas, A. M., J. Horrillo, A. Pampell-Manis, V. Huérfano, and A. Mercado (2015), Advanced tsunami numerical simulations and energy considerations by use of 3D - 2D coupled models: The October 11, 1918, Mona Passage tsunami, *Pure Appl. Geophys.*, *172*(6), 1679–1698.

Lynett, P., and P. L.-F. Liu (2002), A numerical study of submarine-landslide-generated waves and run-up, *Proc. R. Soc. London, Ser. A*, *458*, 2885–2910.

Ma, G., J. T. Kirby, and F. Shi (2013), Numerical simulation of tsunami waves generated by deformable submarine landslides, *Ocean Model.*, *69*, 146–165.

Maretzki, S., S. Grilli, and C. D. P. Baxter (2007), Probabilistic SMF tsunami hazard assessment for the upper east coast of the United States, in *Submarine Mass Movements and Their Consequences*, edited by V. Lykousis, D. Sakellariou, and J. Locat, pp. 377–385, Springer, Netherlands.

Masson, D., C. Habitz, R. Wynn, G. Pederson, and F. Lovholt (2006), Submarine landslides: Processes, triggers and hazard protection, *Philos. Trans. R. Soc. A*, *364*, 2009–2039.

McAdoo, B. G., L. F. Pratson, and D. L. Orange (2000), Submarine landslide geomorphology, US continental slope, *Mar. Geol.*, *169*, 103–136.

Morgenstern, N. R. (1967), Submarine slumping and the initiation of turbidity currents, in *Marine Geotechnique*, edited by A. Richards, pp. 189–210, Univ. of Ill. Press, Urbana.

Nowak, A. S., and K. R. Collins (2000), *Reliability of Structures*, McGraw-Hill, Boston.

Shigihara, Y., and J. Horrillo (2014), A probabilistic methodology for determining tsunami sources generated by submarine landslide— Application to the Gulf of Mexico [in Japanese], *J. Jpn. Soc. Civ. Eng., Ser. B2*, *70*, I_281–I_285.

Stigall, J., and B. Dugan (2010), Overpressure and earthquake initiated slope failure in the Ursa region, northern Gulf of Mexico, *J. Geophys. Res.*, *115*, B04101, doi:10.1029/2009JB006848.

Sue, L. P., R. I. Nokes, and R. A. Walters (2006), Experimental modeling of tsunami generated by underwater landslides, *Sci. Tsunami Hazards*, *24*, 267–287.

Tappin, D. R., P. Watts, and S. T. Grilli (2008), The Papua New Guinea tsunami of 17 July 1998: Anatomy of a catastrophic event, *Nat. Hazards Earth Syst. Sci.*, *8*, 243–266.

ten Brink, U. S., E. L. Geist, and B. D. Andrews (2006), Size distribution of submarine landslides and its implication to tsunami hazard in Puerto Rico, *Geophys. Res. Lett.*, *33*, L11307, doi:10.1029/2006GL026125.

ten Brink, U. S., D. Twichell, P. Lynett, E. Geist, J. Chaytor, H. Lee, B. Buczkowski, and C. Flores (2009a), Regional assessment of tsunami potential in the Gulf of Mexico, U.S. Geol. Surv. Admin. Rep.

ten Brink, U. S., H. J. Lee, E. L. Geist, and D. Twichell (2009b), Assessment of tsunami hazard to the U.S. East Coast using relationships between submarine landslides and earthquakes, *Mar. Geol.*, *264*, 65–73.

Thomopoulos, N. T. (2012), *Essentials of Monte Carlo simulation: Statistical Methods for Building Simulation Models*, 57–70 pp., Springer, N. Y.

Watts, P., S. Grilli, D. Tappin, and G. Fryer (2005), Tsunami generation by submarine mass failure. II: Predictive equations and case studies, *J. Waterw. Port Coastal Ocean Eng.*, *131*, 298–310.

Whitmore, P., U. ten Brink, M. Caropolo, V. Huerfano-Moreno, W. Knight, W. Sammler, and A. Sandrik (2009), NOAA/West Coast and Alaska Tsunami Warning Center Atlantic Ocean response criteria, *Sci. Tsunami Hazards*, *28*, 86–107.